Computational fluid dynamics (CFD) numerical simulation and particle image velocimetry (PIV) measurement of a packed flotation column

Xiaokang Yan [1,2], Zhuying Chen [3], Lijun Wang [2,3]

[1] School of Chemical Engineering and Technology, China University of Mining & Technology, Xuzhou, 221116 Jiangsu, China

[2] National Engineering Research Center of Coal Preparation & Purification, Xuzhou, Jiangsu, China

[3] School of Electrical and Power engineering, China University of Mining & Technology, Xuzhou, 221116 Jiangsu, China

Corresponding author: wanglijun@cumt.edu.cn (Lijun Wang)

Abstract: Packing is a useful method to obtain a static separation environment for a high flotation recovery and selectivity. In this study, the single-phase flow field in a packed lab-scale cyclonic-static microbubble flotation column (FCSMC) was investigated by computational fluid dynamics (CFD) simulation. Turbulence model was verified by Particle Image Velocimetry (PIV) experiment; the simulation results obtained by the RSM (Reynolds Stress Model) are closer to the experimental data. Based on this validation, RSM turbulence model was used to obtain the effect of sieve-plate on the hydrodynamic characteristics in the column flotation zone. The results show that the sieve-plate packing arrangement greatly straightens the rotation flow and decreases the turbulence. To further improve the effect of packing, two layers of sieve plates were used, and one diameter (1D = 190 mm) was selected as the reasonable distance between the two layers of sieve plates. To quantitative evaluate the effect of sieve-plate packing, the logarithm of P_{dk} over the logarithm of P_{do} was calculated based on the volume-averaged turbulence dissipation rate, increasing from 24.72 for one layer of sieve-plate packing to 216.96 for two layers of sieve-plate packing. The probability of detachment significantly decreased for two layers of sieve-plate packing, and the recovery efficiency was significantly improved.

Keywords: cyclonic-static microbubble flotation column, computational fluid dynamics, sieve-plate packing, particle image velocimetry, velocity distribution

1. Introduction

Based on the surface hydrophobicity difference of particles, froth flotation is a widely used separation method in the mineral processing industry (Shean and Cilliers, 2011; Wang et al., 2014). Cyclonic-static microbubble flotation column (FCSMC) integrating multiple mineralization steps has been successfully used for roughing and scavenging in the mineral flotation industry (Zhang et al., 2013). The schematic of an FCSMC is shown as in Fig. 1; it consists of a column flotation unit, cyclone flotation unit, and pipe flotation unit.

The column flotation unit features countercurrent mineralization. When pulp is fed into the column, the falling hydrophobic particles are attached to the ascending bubbles. Then, mineralized bubble–particle aggregates move upwards to the foam layer; in this part, a low turbulent separation environment is needed to ensure a high recovery.

In the cyclone flotation unit, the particles that are detached from the bubbles or not attached with the bubbles before are further mineralized under the high-intensity centrifugal force field. In the pipe flotation unit, when the middlings continuously flows through a circulation pump, the surrounding

air is sucked into the bubble generator and crushed into abundant microbubbles. Then, a more intense turbulent environment is formed and collision probability increased as a result.

To date, extensive studies have been conducted to further improve the superiority of an FCSMC. For example, Wang et al. (2015) investigated the effect of reversal cone angles in a cyclone flotation unit on the flow field and concluded that the vortexes are significantly affected by the angle. Wang et al. (2017) introduced a vortex generator in a pipe flow unit to increase the turbulence dissipation rate, improving the recovery of fine minerals. The flow field in a column flotation unit has also attracted much attention. When a fluid is tangentially injected into a cyclonic flotation unit, an axial vortex is formed in the column without packing (Yan et al., 2012), this causes a turbulent flow field and contradicts the desired static separation in a column flotation unit and becomes a major technical obstacle in the development of cyclonic-static microbubble column flotation (Zhang et al., 2014).

To solve this problem, the flotation column was packed, leading to the tower equipment; it has been proved to be a useful method to improve the flotation recovery (Yang, 1988). For packed flotation, the flow patterns become relatively comlex, the computational fluid dynamics (CFD) is increasingly resorted to study the flow field in the packed equipment (Li et al., 2014; Ma et al., 2015; Rahimi et al., 2012). In the flotation column, Liu et al. (2007) used the Laser Doppler Velocity (LDV) and CFD methods to investigate the velocity field distribution in the sieved flotation column. The results show that the tangential velocity was weakened, and the plug flow environment was strengthened. However, the simulation results could not be validated as the LDV method is too limited to accurately represent the velocity distribution of the flow field. Moreover, Zhang et al. (2017) used a single-phase model to simulate the flow characteristics in a flotation column packed with fluid guiding media. The results show that the detachment probability of particles decreased dramatically, yet, still the results were not validated. To obtain reliable simulation results, the experimental and simulation method should be combined (Zarei et al., 2010; Wang et al., 2015; Zhang et al., 2016). PIV has been used as a nonintrusive velocity field measurement method (Brady et al., 2006; Deng et al., 2013; Yan et al., 2016); it has been first used for the validation of a CFD model (Wang et al., 2015).

In this study, first a single-phase PIV test was conducted for turbulence model validation, and then the effect of sieve-plate on flow field was investigated by numerical simulation. A second sieve plate was introduced at a suitable height to further improve the effect of packing. Finally, the effect of sieve-plate packing was quantitatively compared by counting the detachment probability.
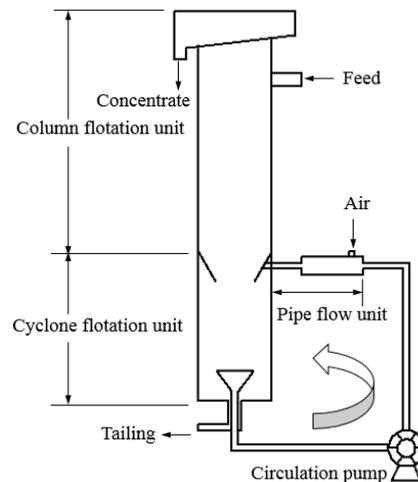

Fig. 1. Schematic of a FCSMC

2. Methodology

2.1 PIV apparatus and experiment

2.1.1 Experimental apparatus

Fig. 2 shows the experimental setup. This includes a PIV system, middlings circulation pump, and a laboratory FCSMC. The 2D PIV system (Dantec's 2D2C DC) consists of a double-pulse laser, sheet

optics, a CCD camera, a synchronous controller, and a Dynamic Studio 3.2 software provided by Dantec; the synchronizer connects both a laser and CCD camera. The camera was placed at a certain distance from the column and perpendicular to the laser.

The laboratory FCSMC has a diameter of 190 mm and a height of 1400 mm. A cube Plexiglas box surrounds the column. The experiment is started by filling the box with water to eliminate refraction from the cylindrical column. The column flotation unit is open (without packing the sieve plates). An inverted cone with two tangential middlings inlets is placed at the middle of the column. A flowmeter is installed in each pipeline, and a valve is used to control the flow rates. The head of the middlings circulation pump (Grundfos CM3-4) is 35 m, and the full flow rate is 5 m³/h.
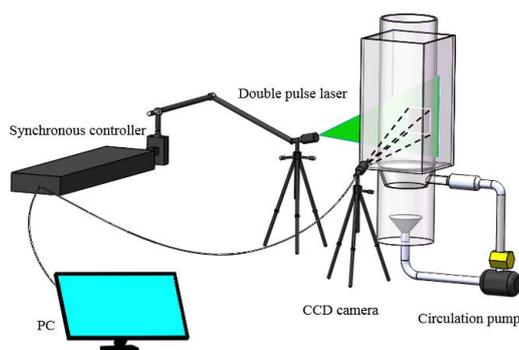

Fig. 2. Experimental setup

2.1.2 PIV experiment

Before the test, water was added to the column until the free liquid level was 300 mm from the top, the laser irradiation on the measured vertical plane, 20 mm to the vertical axis of the column, as shown in Fig. 3(a). Then, the camera was placed at a proper location and perpendicular to the laser, the area covered by the CCD camera spanned about 90 mm (width) × 110 mm (height) as shown in Fig. 3(b). During the test, the circulating flux was maintained at 1.5 m³/h. Polystyrene seeding particles (1.05 g/cm³ in density and 10 μm in size) prepared in advance were added to the column. The laser light reflected from seeding particles was captured using the CCD camera; 500 image pairs were captured at 10 Hz with an exposure time of 200 μs for the camera and a trigger time of 300 μs for the laser. Finally, the average velocity of 500 image pairs was analyzed using a Dynamic Studio software.
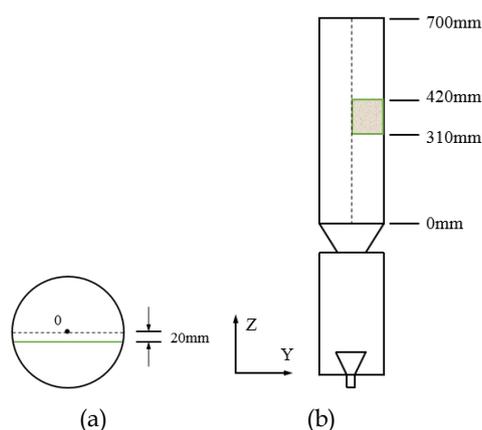

Fig. 3. Schematic of PIV measurement area. (a) Measured plane and (b) measured region

2.2 Numerical methods

2.2.1 Geometrical model

The open FCSMC for simulation is shown in Fig. 4. The difference in the FCSMC configuration between the CFD and experimental model is the absence of a tailings outlet. This is because the outlet

of tailings is closed during the experiment; for simplifying the simulation model, the tailings outlet was removed. Another difference is that the height of column flotation unit was shortened from 1000 mm to 700 mm where free liquid surface locates in the PIV test.
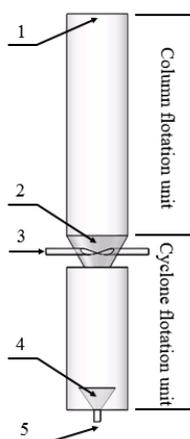

Fig. 4. Schematic diagram of open FCSMC: 1 - concentrate outlet,
2 - cyclonic reversal cone, 3 - middlings inlet, 4 - upright cone, 5 - middlings outlet

2.2.2 Mesh independent

A commercial software ANSYS ICEM CFD (ANSYS Inc., 2012) was used to generate the mesh. Both structured grid and unstructured mesh were used as shown in Fig. 5.
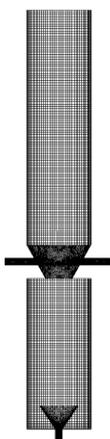

Fig. 5. Mesh of the open FCSMC column

A mesh independence test was carried out for the open FCSMC, and the volume-averaged turbulence dissipation rate of the column flotation zone was selected as the principle criterion. Table 1 shows the dependence of quantities on the grid size. After 366894 cells, a further increase in cells resulted in less than 1% variation in the volume-averaged turbulence dissipation rate. Considering both the accuracy of simulation and computational cost, the following simulations were performed with 366894 cells of the open FCSMC.

Table 1. Volume-averaged turbulence dissipation rate for various numbers of cells

Cells	123817	170620	246943	366894	463268
Volume-averaged turbulence dissipation rate (m^2/s^3)	0.00101	0.00107	0.00115	0.00119	0.00118

2.2.3 Verification of numerical methods

SIMPLE algorithm was used for the pressure–velocity coupling scheme. A second-order upwind scheme was used in the momentum discretization, and PRESTO! scheme was used for pressure discretization. The boundary conditions were defined based on the PIV experiment, they are shown in Table 2.

Table 2. Simulation boundary conditions

Boundary name	Boundary type	Boundary value
Middlings inlet	Velocity inlet	0.67 m/s
Middlings outlet	Velocity inlet	–1.34 m/s
Concentrate outlet	Symmetry	

To verify the accuracy of the numerical model, three different turbulence models, Standard k-ε, Realizable k-ε and RSM turbulence model were compared with PIV test results. The velocity profiles of the line located at z = 365 mm and 20 mm to the column vertical axis are shown in Fig. 6. It is obvious that the value of RSM turbulence model ate closer to PIV experimental data. Therefore, the RSM turbulence model is more suitable for the FCSMC column in this study, and the rest of the simulation was also performed using the RSM turbulence model.
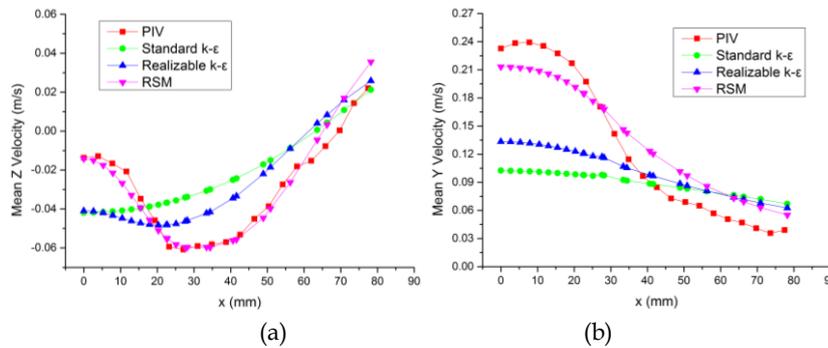

(a) (b)

Fig. 6. Velocity distribution on line z = 365 mm (y = 20 mm); (a) mean axial velocity and (b) mean radial velocity

2.2.4 Governing equations

In this study, the flow is considered as incompressible, three dimensional, and in the transient state, and the RSM turbulence model based on the Reynolds-averaged Navier–Stokes (RANS) approach was used. The governing equations are as follows:

Continuity equation:

$$\frac{\partial u_i}{\partial x_i} = 0 . \tag{1}$$

Momentum equation:

$$\frac{\partial(\rho u_i)}{\partial t} + \frac{\partial}{\partial x_i}(\rho u_i u_j) = -\frac{\partial p}{\partial x_i} + \frac{\partial}{\partial x_i}\left[\mu(\frac{\partial u_i}{\partial x_j} + \frac{\partial u_j}{\partial x_i})\right] + \frac{\partial}{\partial x_j}(-\overline{u_i' u_j'}) \tag{2}$$

Transport equation:

$$\frac{\partial}{\partial t}(\rho \overline{u_i' u_j'}) + \frac{\partial}{\partial x_k}(\rho u_k \overline{u_i' u_j'}) = D_{T,ij} - \rho(\overline{u_i' u_k'}\frac{\partial u_j}{\partial x_k} + \overline{u_j' u_k'}\frac{\partial u_i}{\partial x_k}) + \overline{p'(\frac{\partial u_i'}{\partial x_j} + \frac{\partial u_j'}{\partial x_i})} - 2\mu\overline{\frac{\partial u_i'}{\partial x_j}\frac{\partial u_j'}{\partial x_i}} , \tag{3}$$

where turbulent diffusion $D_{T,ij}$ is:

$$D_{T,ij} = -\frac{\partial}{\partial x_k}\left[\rho\overline{u_i'u_j'u_k'} + \overline{p'(\delta_{kj}u_i' + \delta_{ik}u_j')}\right].\qquad(4)$$

In these equations, u is the mean velocity; u' is the fluctuating velocity; the subscripts i and j are 1, 2, or 3 and represent x, y, or z components. μ is the dynamic viscosity, ρ is the fluid density, and δ is the Kronecker delta function, p is the pressure, and $\overline{u_i'u_j'}$ is the Reynolds stress tenser.

3. Results and discussion

3.1 Flow field in FCSMC without filling

Fig. 7 shows the streamlines in the open column, and the mean x and z velocity distribution are shown in Fig. 8. As shown in Figs. 7 and 8, when the fluid is tangentially injected through the middlings inlet to the cyclonic flotation unit, the reversal cone induces a rotation and lifting effect on the fluid. Then, the fluid is divided into two parts: One part moves upwards, and another part mixes with the spiraling down fluid moving downwards.
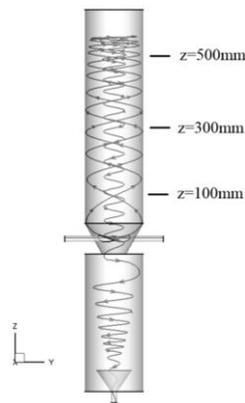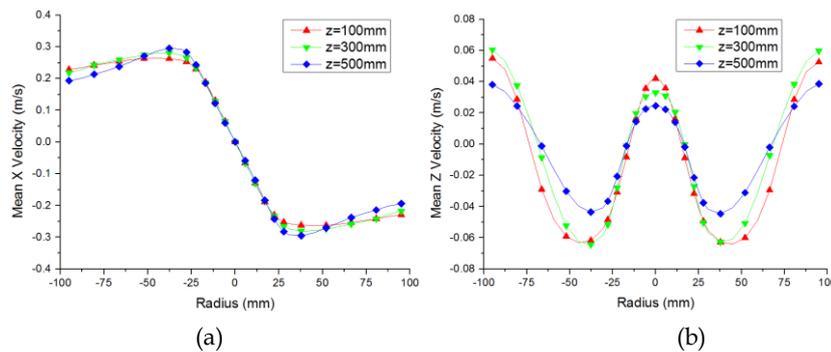

Fig. 7. Streamline in the open FCSMC

Fig. 8. Velocity distribution within the column flotation unit at different heights. (a) Mean tangential velocity and (b) mean axial velocity.

In the column flotation unit, the fluid pattern can be divided into three parts, and each part corresponds to one type of vortex along the radial direction. The first part is 0–20 mm, and a quasi-forced vortex is formed near the center line of the column and spring up with a lower speed. The tangential and axial velocities range from 0–0.3 m/s and 0–0.04 m/s, respectively. The second part is 20–70 mm. In this part, the fluid springs down from the free surface to the tailing outlet because of suction force from the circulation pump. The tangential and axial velocities range from 0.25–0.3 m/s and 0–0.06 m/s, respectively. The third part is 70–95 mm. In this part, the fluid springs up near the wall, and the tangential and axial velocities range from 0.2–0.25 m/s and 0–0.06 m/s, respectively.

In the column flotation unit, the tangential velocity approximately remains unchanged at different heights. However, from the center to the wall, the tangential velocity first increased from 0–0.3 m/s and then remained at a high value. A high swirling intensity appeared at the near-wall region range 25–95 mm along the radial direction. Moreover, the axial velocity direction was unpredictable in the column flotation unit. From the center to the wall, first it showed a positive to negative direction change and then changed to a positive direction again.

Particle size is an important factor affecting the flotation recovery. The fine particles with a low inertia show low recovery rates owing to decreased collision efficiencies (Miettinen et al., 2010). In contrast, coarse particles frequently collide with the bubbles because of a higher inertia. The recovery rates are mainly determined by the stability of bubble–particle aggregates. In the highly turbulent environment of a flotation cell, the stability of coarse particles is relatively low owing to the disruption of bubble–particle aggregates (Feng and Aldrich, 1999; Jameson, 2010). Therefore, in the column flotation zone, a low turbulent separation environment is needed to reduce the detachment probability for the floatation of coarse particles. In addition, a low-speed flow field in which the bubbles move upwards under buoyancy and the particles move downwards under gravity is also crucial to achieve countercurrent mineralization. To achieve this goal, sieve-plate packing was introduced in the next part.

3.2 Effect of sieve-plate packing

The configuration of one layer of sieve-plate packing is shown in Fig. 9 (a). The sieve plate was installed in the column flotation zone, and the distance between the bottom surface of the sieve plate and base of the column flotation zone (z = 0 mm) is 0.1D (19 mm). The sieve plate used in this study is shown in Fig. 9 (b). The diameter of the sieve plate is 190 mm; the thickness and pore diameter are 5 mm and 10 mm, respectively. The porosity is 52.6%.
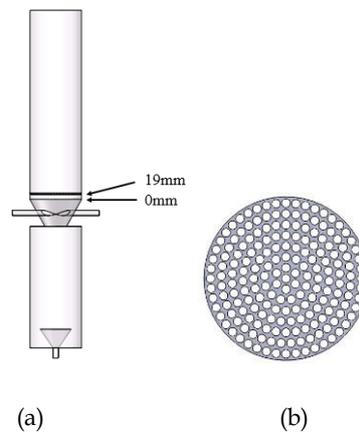

(a)　　　　　　　(b)

Fig. 9. Schematic of sieve-plate packing. (a) Configurations of one layer of sieve-plate packing and
(b) geometry of the sieve plate.

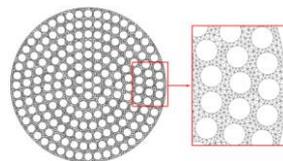Unstructured mesh (as shown in Fig. 10) was used due to the complex structure of the sieve plate.

Fig. 10. Schematic of sieve-plate mesh

To highlight the effect of sieve plate, the contour of the mean axial velocity at x = 0 mm plane is shown in Fig. 11. Compared to the open column, the sieve-plate packing significantly affected the flow field. The spring up vortex in the center disappeared after the packing, and the magnitude of velocity above the sieve plate also decreased. However, the back-mixing still exists in the column flotation

unit, indicating that one layer of sieve plate is not enough to create the desired separation environment. To further enhance the efficiency of sieve plate, a second layer of sieve plate was used in the next part.
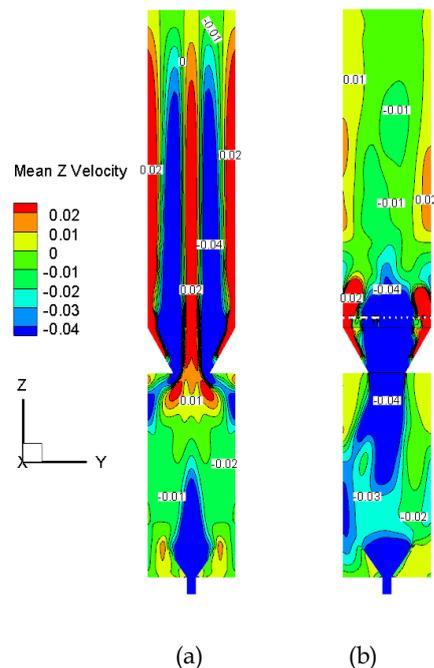

(a)   (b)

Fig. 11. Contour of mean z velocity on plane of $x = 0$ mm. (a) Open column and (b) one layer of sieve-plate packing

3.3 Two layers of sieve-plate packing

To determine a suitable distance between the two layers of sieve plates, the tangential velocity along the axial direction from $z = 50$–700 mm of one layer of sieve-plate packing is shown in Fig. 12.
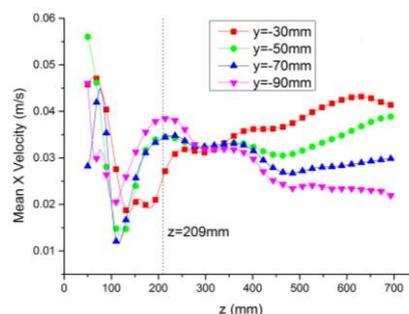

Fig. 12. Tangential velocity distribution along the axial direction on the iso-surface of $y = -90$ mm, -70 mm, -50 mm, -30 mm ($x = 0$ mm, $z = 50$–700 mm)

Apparently, in the range of $z = 50$–120 mm, the tangential velocity dramatic decreased with the increase in height and reached a minimum value. In the range of $z = 120$–209 mm, the tangential velocity increased and remained at a high value at $z = 209$ mm. It can be concluded that the effect of sieve plate is limited, and this range is about one diameter of the column after the first sieve plate. Therefore, 1D (190 mm) was selected as the distance between the sieve plates, i.e., the bottom surface of the second sieve plate was arranged at $z = 209$ mm as shown in Fig. 13.

Fig. 14 shows a comparison of the velocity distribution at $z = 365$ mm ($x = 0$ mm) of the open FCSMC and two types of sieve-plate packing model. Two layers of sieve-plate packing made the velocity distribution more uniform, and the rotation flow approximately disappeared above the second sieve plate. The desired plug flow conductive the separation efficiency was achieved.
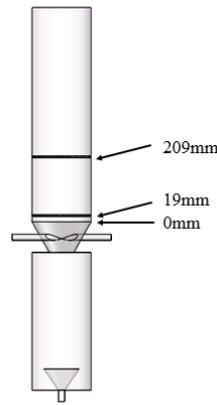
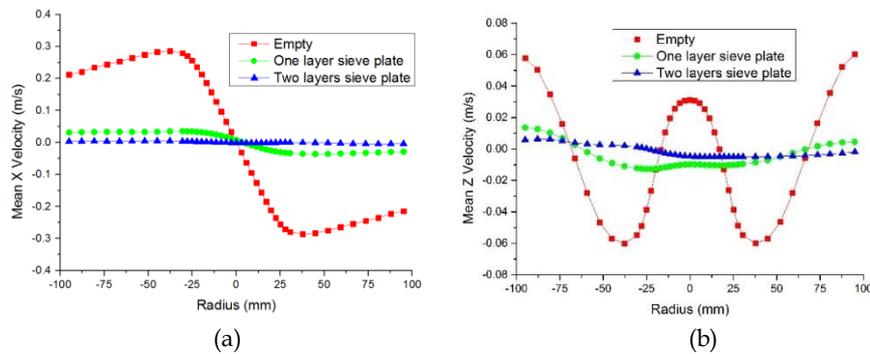Fig. 13. Configurations of two layers of sieve-plate packing

Fig. 14. Velocity distribution at z = 365 mm (x = 0). (a) Mean x velocity and (b) mean z velocity

3.4 Probability of detachment

The ultimate aim of sieve-plate packing is to straighten the turbulent flow in the column flotation unit to achieve a static flow, in which the bubble–particle aggregates cannot easily detach from each other. Many models have been developed to quantify the detachment rate in a turbulent flow field (Goel and Jameson, 2012; Schulze, 1982). Wang et al. (2014) compared the detachment models obtained by (Sherrell, 2004) with the experimental results reported by (Goel and Jameson, 2012). The results show that the detachment rate at a low turbulence level is very different from the experimental results. Considering that the detachment probability is an exponential function of energy dissipation rate and increases with turbulence level, a new model consistent with the experimental results is proposed as follows (Wang et al., 2014):

$$P_d = \exp\left(-\frac{8\sigma R_p^2 (1-\cos\theta)^2}{c_2 \rho_l \varepsilon^{2/3} d_p^{11/3}}\right) , \tag{5}$$

where σ is the liquid surface tension; θ is the contact angle; ρ_l is the liquid density; R_p and d_p are the radius and diameter of the particles, respectively; c_2 is a constant with a value of 0.73.

To quantify the effect of sieve-plate packing, Eq. 5 can be simplified to:

$$\frac{\ln P_{dk}}{\ln P_{do}} = \left(\frac{\varepsilon_o}{\varepsilon_k}\right)^{2/3} , \tag{6}$$

where P_{d0} is the detachment probability of the open column, P_{dk} is the detachment probability of the column filled with k layer(s) of sieve plates.

The volume-averaged turbulence dissipation rate (ε_k) in the column flotation unit varied from z = 300 mm to z = 700 mm in the open column (ε_0). The one layer of sieve-plate packing (ε_1) and two

layers of sieve-plate packing (ε_2), ε_0=0.0009587, ε_1=0.0000078, ε_2=0.0000003 m²/s³, respectively. Using Eq. 6, $\ln P_{d1}/\ln P_{d0} = 24.72$ and $\ln P_{d2}/\ln P_{d0} = 216.96$. It can be concluded that two layers of sieve-plate packing is more efficient than one layer of sieve-plate packing, and the probability of detachment significantly decreases in two layers of sieve-plate packing arrangement case. Packing is an effective way for improving the flotation performance.

4. Conclusions

(1) A single-phase model was used to investigate the flow field in FCSMC, and a PIV test in the open laboratory FCSMC was carried out to validate the turbulence model. The results show that the simulation results obtained by the RSM turbulence model are closer to the experimental data.

(2) In the open flotation column, the simulation results show that three types of vortex exist in the column flotation unit, and the axial back-mixing is prominent.

(3) To straighten the irregular flow pattern, a sieve-plate packing method is proposed. Under the effect of sieve plate, both the tangential and axial velocities decreased in the column flotation unit. With one layer of sieve-plate packing, the axial vortex still exists on the sieve plate.

(4) To further strengthen the effect of sieve plate, a second sieve plate was installed above the first sieve plate at 190 mm. The results show that the flow field became more close to the plug flow, achieving a static flow.

(5) To quantitatively evaluate the effect of sieve-plate packing, $\ln P_{dk}$ over $\ln P_{d0}$ was calculated based on the volume-averaged turbulence dissipation rate, increasing from 24.72 in one layer of sieve-plate packing to 216.96 in two layers of sieve-plate packing. The probability of detachment significantly decreased by using two layers of sieve-plate packing, and the recovery efficiency was improved.

References

ANSYS INC., 2012. ANSYS ICEM CFD User Manual.

BRADY, M.R., TELIONIS, D.P., VLACHOS, P.P., YOON, R.-H., 2006. *Evaluation of multiphase flotation models in grid turbulence via Particle Image Velocimetry*. International Journal of Mineral Processing, 80(2-4), 133-143.

DENG, X., LIU, J., WANG, Y., CAO, Y., 2013. *Velocity distribution of the flow field in the cyclonic zone of cyclone-static micro-bubble flotation column*. International Journal of Mining Science and Technology, 23(1), 89-94.

FENG, D., ALDRICH, C., 1999. *Effect of particle size on flotation performance of complex sulphide ores*. Minerals Engineering, 12(7), 721-731.

GOEL, S., JAMESON, G.J., 2012. *Detachment of particles from bubbles in an agitated vessel*. Minerals Engineering, 36-38, 324-330.

JAMESON, G.J., 2010. *Advances in fine and coarse particle flotation*. Canadian Metallurgical Quarterly, 49(4), 325-330.

LI, Q., LI, L., ZHANG, M., LEI, Z., 2014. *Modeling Flow-Guided Sieve Tray Hydraulics Using Computational Fluid Dynamics*. Industrial & Engineering Chemistry Research, 53(11), 4480-4488.

LIU, J., ZHANG, M., LIU, H., WANG, Y., CHEN, J., 2007. *Velocity field distribution of flotation fluid in the sieved-flotation column*. Journal of China University of Mining & Technology 36(5), 578.

MA, Y., JI, L., ZHANG, J., CHEN, K., WU, B., WU, Y., ZHU, J., 2015. *CFD gas–liquid simulation of oriented valve tray*. Chinese Journal of Chemical Engineering, 23(10), 1603-1609.

MIETTINEN, T., RALSTON, J., FORNASIERO, D., 2010. *The limits of fine particle flotation*. Minerals Engineering, 23(5), 420-437.

RAHIMI, R., MAZAREI SOTOODEH, M., BAHRAMIFAR, E., 2012. *The effect of tray geometry on the sieve tray efficiency*. Chemical Engineering Science, 76, 90-98.

SCHULZE, H.J., 1982. *Dimensionless number and approximate calculation of the upper particle size of floatability in flotation machines*. International Journal of Mineral Processing, 9(4), 321-328.

SHEAN, B.J., CILLIERS, J.J., 2011. *A review of froth flotation control*. International Journal of Mineral Processing, 100(3-4), 57-71.

SHERRELL, I.M., 2004. *Development of a Flotation Rate Equation from First Principles under Turbulent Flow Conditions*. Virginia Tech.

WANG, A., YAN, X., WANG, L., CAO, Y., LIU, J., 2015a. *Effect of cone angles on single-phase flow of a laboratory cyclonic-static micro-bubble flotation column: PIV measurement and CFD simulations*. Separation and Purification Technology, 149, 308-314.

WANG, G., ZHOU, S., JOSHI, J.B., JAMESON, G.J., EVANS, G.M., 2014. *An energy model on particle detachment in the turbulent field*. Minerals Engineering, 69, 165-169.

WANG, L., JIA, Y., YAN, X., ZHOU, C., 2015b. *Gas-liquid numerical simulation on micro-bubble generator and optimization on the nozzle-to-throat spacing*. Asia-Pacific Journal of Chemical Engineering, 10(6), 893-903.

WANG, L., WANG, Y., YAN, X., WANG, A., CAO, Y., 2017. *A numerical study on efficient recovery of fine-grained minerals with vortex generators in pipe flow unit of a cyclonic-static micro bubble flotation column*. Chemical Engineering Science, 158, 304-313.

YAN, X., LIU, J., CAO, Y., WANG, L., 2012. *A single-phase turbulent flow numerical simulation of a cyclonic-static micro bubble flotation column*. International Journal of Mining Science and Technology, 22(1), 95-100.

YAN, X., SHI, R., XU, Y., WANG, A., LIU, Y., WANG, L., CAO, Y., 2016. *Bubble behaviors in a lab-scale cyclonic-static micro-bubble flotation column*. Asia-Pacific Journal of Chemical Engineering, 11(6), 939-948.

YANG, D.C., 1988. *A new packed column flotation system*. Column flotation, 88, 257-265.

ZAREI, T., RAHIMI, R., ZIVDAR, M., 2010. *Computational fluid dynamic simulation of MVG tray hydraulics*. Korean Journal of Chemical Engineering, 26(5), 1213-1219.

ZHANG, H., LIU, J., WANG, Y., CAO, Y., MA, Z., LI, X., 2013. *Cyclonic-static micro-bubble flotation column*. Minerals Engineering, 45, 1-3.

ZHANG, L., LI, Z., YANG, N., JIANG, B., CONG, H., ZHANG, Z., 2016. *Hydrodynamics and mass transfer performance of vapor–liquid flow of orthogonal wave tray column*. Journal of the Taiwan Institute of Chemical Engineers, 63, 6-16.

ZHANG, M., LI, T., WANG, G., 2017. *A CFD study of the flow characteristics in a packed flotation column: Implications for flotation recovery improvement*. International Journal of Mineral Processing, 159, 60-68.

ZHANG, M., MA, S., SHEN, J., LIU, D., 2014. *Study on Mixed Packing of Flotation Column*. International Conference on Mechatronics, Electronic, Industrial and Control Engineering (MEIC 2014).